ANALYSIS OF SPACEBORNE HYPERION IMAGERY FOR THE ESTIMATION OF FRACTIONAL COVER OF RANGELAND ECOSYSTEMS

Jinkai Zhang [a, *], Karl Staenz[a,b], Peter R. Eddy[a,d], Nadia Rochdi[a], Dave Rolfson[b], Anne M. Smith[c]

[a]Alberta Terrestrial Imaging Center, 401, 817-4th Avenue S., Lethbridge, AB, T1J 0P3, Canada
[b] Canada and Department of Geography, University of Lethbridge, 4401 University Drive, Lethbridge, AB, T1K 3M4, Canada
[c]Agriculture and Agri-Food Canada, Lethbridge Research Center, 5403 1st Avenue S., Lethbridge, AB, T1J 4B1, Canada
[d]Iunctus Geomatics Corp., 401, 817-4th Avenue S., Lethbridge, AB, T1J 0P3, Canada

KEY WORDS: Rangeland, Hyperspectral, Endmember, Spectral Unmixing

ABSTRACT:

The goal of this research was to investigate the potential of hyperspectral Hyperion (EO-1) data to derive fractional cover of rangeland components using constrained linear spectral mixture analysis. Hyperion image data were acquired over the Antelope Creek Ranch located in southern Alberta, Canada in July 2005. These image data were first corrected for the sensor artifacts such as spatial mis-registration between the VNIR and SWIR data and striping. These data were then atmospherically corrected and transformed to surface reflectance, corrected for sensor smile/frown and post-processed to remove residual errors. Iterative Error Analysis was utilized to find image endmembers that acted as inputs to the constrained spectral unmixing. The preliminary results show that spectral unmixing was promising for percent cover estimation of green vegetation and litter/soil, but separation of green grass from green shrub was challenging due to their spectral similarity.

1. INTRODUCTION

Rangeland occupies 47% of the Earth's land surface and represents a major source of livestock food production (Holechek, et. al., 1989). Effective rangeland management techniques are crucial to sustain soil quality, enhance the availability of clean water, sequester excess carbon dioxide and maintain biodiversity in the rangeland ecosystem. There is an urgent need for timely information on the state of rangeland for the protection and long-term sustainability of this ecosystem. Amongst indicators for monitoring rangeland ecosystems, vegetation cover and condition are very important parameters for understanding the dynamics of plants in such an environment [Rowe, et.al., 2002].

Due to the extensive nature of rangeland, satellite remote sensing provides the means to map fractional cover on a regional basis in a cost-effective and timely manner. By providing image data in hundreds of contiguous narrow spectral bands, hyperspectral imaging allows the extraction of laboratory-like spectra for each pixel in the image. This high level of spectral detail provides a rich source of compositional information about the targets, making it feasible to identify subtle differences between vegetation communities. Several studies have demonstrated the capability of airborne hyperspectral remote sensing to detect and map vegetation species and their fractional cover (Asner, et al., 2002; Lass, et al., 2005). However, such data are not sufficient for monitoring rangeland on an operational basis due to their relatively high cost and low spatial coverage. Operational spaceborne hyperspectral satellites, such as the approved German EnMAP mission, will provide the data necessary to support and improve sustainable rangeland management practices.

A quantitative approach, spectral mixture analysis (SMA), is commonly used to determine the fractional cover on a pixel basis from hyperspectral data. The key task in SMA is to define a set of "pure" endmembers that are relevant to the mapping objectives and are representative of the physical components of the surface. For rangeland monitoring, these endmembers could be different plant species/communities, shrub, soil, shadow and other surface components (e.g., plant litter, lichens, and rocks). Endmembers can be derived from the imagery (image endmembers) or measurements in the laboratory/field (library endmembers). Image endmembers are commonly preferred over the use of library endmembers because the latter are not always available, and if available, they are not necessarily acquired under the same conditions as airborne or satellite image data and may not be representative of true image components.

The selection of image endmembers is typically achieved through the implicit (Pixel Purity Index (Boardman, et. al., 1995)) or explicit use of convex geometry. A simplex is fit to the convex hull of the n-dimensional data cloud and the vertices of the simplex define the spectral properties of the endmembers. Although a number of approaches to define endmembers have been the focus of recent research efforts and several methodologies (e.g., Iterative Error Analysis (Neville, et. al., 1999), N-FINDR (Winter, 1999), Sequential Projection Algorithm (Zhang, et. al., 2008), Vertex Component Analysis (VCA) (Nascimento and Dias, 2005), Sequential Maximum Angle Convex Cone (SMACC) (Gruninger, et. al., 2004), Iterated Constrained Endmembers (ICE) (Berman, et. al., 2004), Simplex Growing Algorithm (SGA) (Chang, et al., 2006) and

* Corresponding author. Jinkai Zhang <jinkai.zhang@imagingcenter.ca>.

Minimum Volume Constrained Non-Negative Factorization (MVC-NMF) (Miao and Qi, 2007) have been developed, they are seldom tested on rangeland. Identification of suitable endmembers for the subsequent fractional cover estimate in the rangeland system remains unresolved due to its heterogeneity and high spectral similarity amongst vegetative species.

The paper describes in detail the evaluation of automatic endmember selection procedures and subsequent linear SMA in rangeland ecosystems using Hyperion hyperspectral data. The Iterative Error Analysis (IEA) method was selected to automatically find endmembers, given that IEA has been reported as the most robust convex-based algorithm (Plaza, et. al., 2004.). The spatial distribution of percentage cover of major rangeland components, derived from spectral unmixing, will be discussed. Special emphasis is given to the evaluation of the data quality prior to the aforementioned analysis. In particular, spatial and spectral distortions, noise, and striping of the data are investigated and corrected to obtain the best possible data quality, an essential requirement for spectral unmixing techniques.

2. STUDY SITE

The Antelope Creek Ranch (Lat. 50°37′N, Long. 112°10′W, Elevation ~750 m), approximately 15 km west of Brooks, Alberta, Canada was selected as the study site. This site, established in 1986, is a multi-disciplinary, multi-agency research site. The primary objectives of the ranch are to manage the ecosystem in such a way that productive plant cover is available to livestock and wildlife, and that there is adequate nesting cover for waterfowl. The ranch serves as a demonstration to producers and resource managers in the dry mixed-grass region for range improvement through specialized grazing systems which benefits both livestock and wildlife. Figure 1 shows the geographic location of the test site and a natural colour composite from Hyperion data of that site. The rectangular and circular areas are crop land while the white pixels represent exposed soil and litter. Approximately 80% of the subset image is native rangeland.

Figure 1 Location and overview of the study site

3. DATA ACQUISITION AND PROCESSING

3.1 Hyperion data

The hyperspectral data for this study were acquired on July 18, 2005 with the experimental Hyperion sensor on NASA's EO-1 platform. Hyperion is a pushbroom imaging spectrometer that collects data in the along-track direction. This sensor collects the upwelling radiance in 242 spectral bands with a spectral resolution of around 10nm. Hyperion has a single telescope and consists of two spectrographs, one covering the visible and near-infrared (VNIR) wavelength range from 357 nm to 1055 nm, and a second which covers the short-wave infrared (SWIR) from 851 nm to 2576 nm. The spatial resolution of these data are 30m.

3.2 Data preprocessing

The Hyperion EO-1 data were pre-processed with the goal to correct for sensor artifacts and atmospheric effects using the Imaging Spectrometer Data Analysis System (ISDAS) developed at the Canada Centre for Remote Sensing (Figure 2). The first step aligns the SWIR data, correcting for a single pixel offset between the left and right halves of the image in the along-track direction. Once VNIR and SWIR data are aligned, image striping and pixel–column dropouts were removed using the spectral moment matching approach (Sun, et. al., 2008). The VNIR data were then rotated by an angle of 0.22° to match the SWIR data using bi-cubic resampling, and noise was reduced through spectrally constrained averaging.

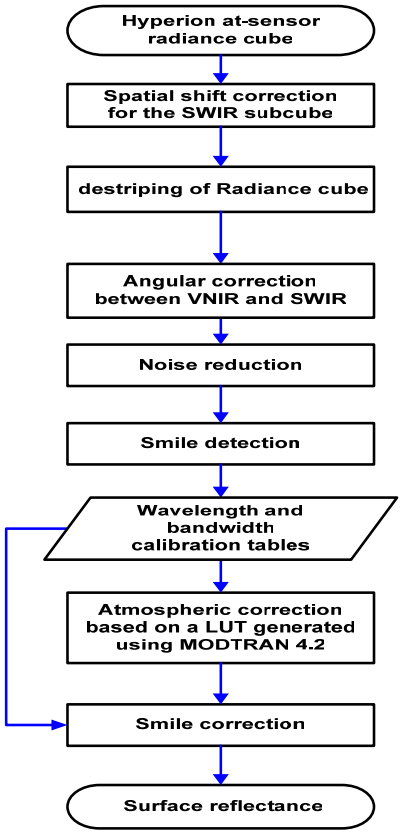

Figure 2 Flow chart for Hyperion data preprocessing

The data cube was subsequently analyzed to characterize the spectral shift ('smile/frown') using atmospheric feature matching. At this step, the data were cropped to exclude noisy bands resulting in a final data set that spans the spectral range from 426.82 nm to 2355.20 nm with a total of 192 bands (excluding the bands in the overlap region between the VNIR and SWIR spectrographs). A method developed by Neville *et al.* (2008) was applied to determine the smile/frown using known atmospheric absorption features. Wavelength shifts (smile/frown effect) were calculated, showing shifts of approximately between 1 and 3 nm across track in the VNIR and SWIR, respectively. The calibrated at-sensor radiance data were converted to surface reflectance using a MODTRAN look-

up table (LUT) approach (Staenz and Williams, 1997). These reflectance data were then corrected for wavelength shift using a spectral resampling technique to achieve a set of common band wavelength centres and bandwidths for the entire data cube. The final post-processing step involved removing residual errors that remained after the correction of sensor artifacts and atmospheric effects (Staenz, et. al., 1999).

4. SPECTRAL UNMIXING AND ENDMEMBER SELECTION

SMA assumes that the pixel-to-pixel variability in a scene results from varying abundances of spectral endmembers. It follows that the spectral response for each pixel is a linear combination of endmember spectra, weighted by their fractional abundances. Let $\vec{p}_{(i,j)}$ denote the spectrum for the pixel in the image coordinates (*i, j*), the foundation of linear constrained SMA (LCSMA) can be defined by the following formulation:

$$\vec{p}_{(i,j)} = \sum_{k=1}^{m} f_{(i,j)k}\vec{e}_k + \vec{\varepsilon}_{(i,j)} \quad (1)$$

$$0 \le f_{(i,j)k} \le 1.0, \quad k = 1,\cdots,m\,; \quad \sum_{k=1}^{m} f_{(i,j)k} = 1 \quad (2)$$

where m is the number of endmembers, $\vec{e}_k$ is the *kth* endmember, $\vec{\varepsilon}_{(i,j)}$ is the error term (residual), which could be due to the noise in the data or due to modeling error (or both), and $f_{(i,j)k}$ is the fractional abundance for the *k*th endmember of pixel (*i, j*). Assuming that the number of endmembers and their spectral signatures are known, the fractional abundances of endmembers in a given pixel are typically determined from a least squares fit (Shimabukuro and Smith, 1991).

The Iterative Error Analysis (IEA), implemented in the Imaging Spectrometer Data Analysis System (ISDAS), was used to automatically find endmembers in the hyperspectral scene. IEA is based on the residual error image generated when a data set is unmixed using a Weighted Non-negative Least Squares approach. To start, the average spectrum of the scene is used to unmix the dataset. When a dataset is unmixed, a residual error image is produced. These errors are calculated using a least-square estimate between the average spectrum and the spectrum of each pixel. These errors are also a measure of the distance between the average spectrum and all the spectra of the dataset. The next step is to find the pixel or pixels that encompass the largest errors, i.e., that are furthest away from the average spectrum. The user provides the number of pixels forming these endmembers. This new endmember is then used to unmix the image cube, and the average spectrum is discarded. The errors will again be used to find the furthest pixels from the first endmember and will create the second endmember. This process is repeated until the number of endmembers pre-determined by the user is reached.

The full spectral range of the Hyperion sensor (except the bands close to water absorption features around 1400nm and 1900nm) was utilized for endmember selection and subsequent unmixing. The IEA technique was used to extract 30 endmembers, each composed of a maximum of 10 pixels. These endmembers were assessed visually and noisy endmembers, due to bad pixels, were discarded. Only error-free endmembers were used in the spectral unmixing (Figure 3)

5. RESULTS AND DISCUSSIONS

5.1 Endmembers

5.1.1 Water/shade: The water/shade endmembers were characterized by a higher reflectance in visible bands and very low reflectance value in the SWIR bands (greater than 1400nm) (Figure 3D). Depending on the depth of the water body, the reflectance varied from 25% to 7% in the green (~550nm) to red (~640nm) spectral regions.

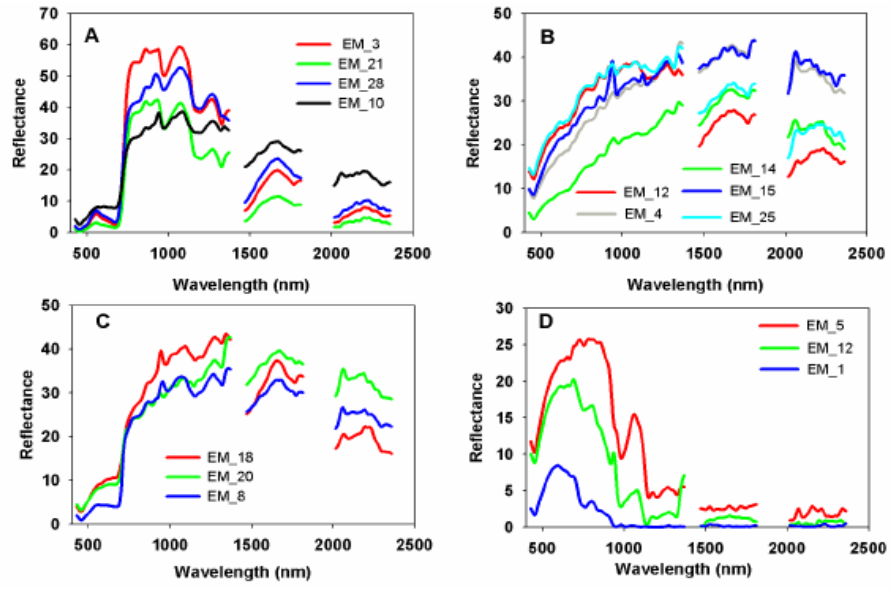

Figure 3 Endmembers used in the spectral unmixing

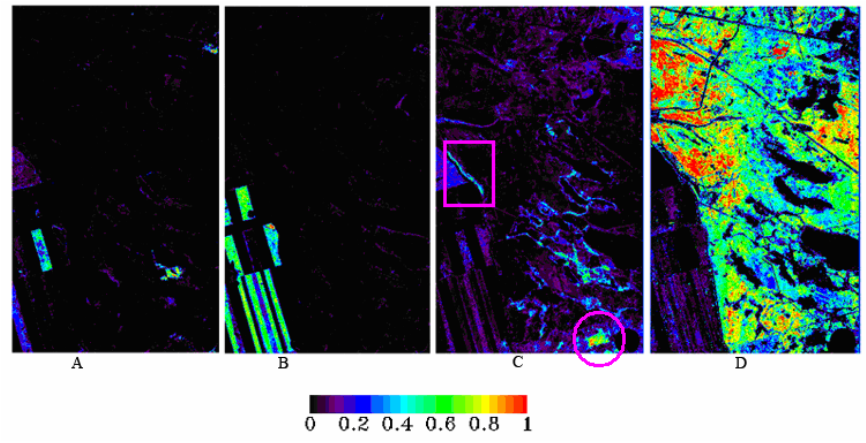

Figure 4 Fractional maps for green vegetation (EM_3, EM_21, EM_28, EM_10)

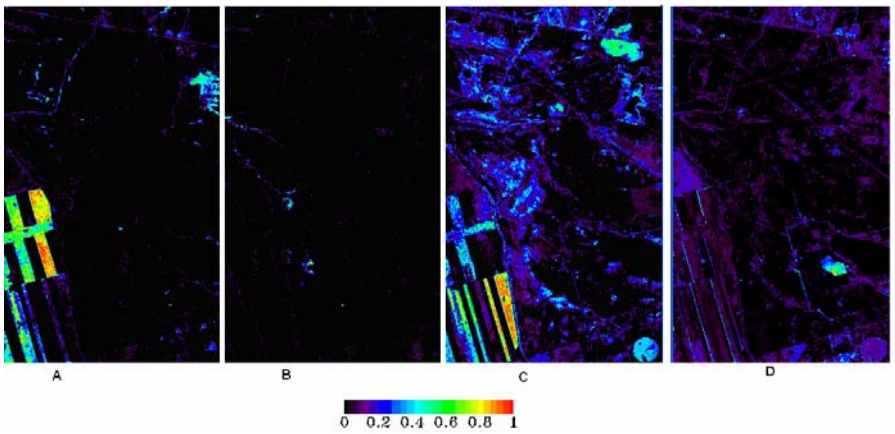

Figure 3 Fractional maps for soil/litter endmembers and yellow grass
A: EM_4; B: EM_12, C: EM_14,
D: total fraction for EM_18, EM_20 and EM_8

5.1.2 .Green vegetation: This group was characterized by typical vegetation absorption features due to photosynthetic pigments and water (Figure 3A). The variability at the green peak (~550nm), chlorophyll absorption (680nm) and water absorption features (945nm and 1190nm) result from the variation of pigment, water content and the leaf structural components. These differences may be attributed to different species or variation in health or phenological stage within species. The detailed characteristics and identification of these endmembers require extensive field validation planned for 2008.

5.1.3 Soil/litter: This rangeland site has been extensively managed resulting in very high litter content and minimal soil exposure, preventing identification of pure soil pixels by the IEA. Therefore, this group of endmembers were defined as mixtures of soil and litter (Figure 3B). Overall, there are no obvious features in the VNIR spectral region except the weak chlorophyll absorption feature and the residual errors from the atmospheric correction around the water absorption bands at 940nm and 1130nm. Depending on the content of litter in the pixel, the spectra vary considerably in the SWIR bands. For example, one of the endmembers has a small clay feature near 2200nm while other endmembers only display the cellulose-related features at 2100nm and 2300nm.

5.1.4 Yellow grass: Compared to green vegetation shown in Figure 3A, the chlorophyll absorption of yellow/scenecent grass endmembers were weaker, and features at 2100nm and 2300nm were distinct due to cellulose (Figure 3C). The spectral shape, cellulose related features and the depth of the chlorophyll absorption could be attributed to the senescent stage of the grass in these endmembers.

5.2 Fractional maps

Figure 4 shows four fractional maps for the green vegetation endmembers. Based on the spatial distribution of the four endmembers, endmembers 3 (Figure 4A) and 21 (Figure 4B) represent two different crop types. Personal communication with domain experts identified that endmember 28 represented areas of irrigated crested wheatgrass (Figure 4C circle) and tree lines (Figure 4C square). Endmember 10 represented the grass/shrub component. Due to the small percentage cover of the shrub and the spectral similarity between the green grass and green shrub leaves, the differentiation of species (green grass and shrub) is very challenging.

The distribution of soil/litter is relatively low except within the cultivated agricultural land as shown in the bottom left corner of Figure 5A and Figure 5C. The overall soil/litter percentage is less than 25% of the total rangeland cover due to the dominant

green vegetation in the peak growing season. The detailed interpretation of these maps requires further analysis and field work.

The fraction cover for the yellow/scenecent grass endmembers was very limited (Figure 5D). This fractional map is the sum of three endmembers shown in Figure 3C. Since these hyperspectral data were acquired in July (close to peak growing season) grass senescence may not have started. There is a patch where the abundance of yellow grass is around 40% in the bottom right quarter. The identification of this patch requires field work which will be conducted this summer.

6. CONCLUSION AND RECOMMENDATIONS

A preliminary investigation indicates that endmember analysis of hyperspectral data and spectral mixture analysis shows potential for the estimation of the fractional cover of rangeland components. However, it was found that two important factors impede the automatic endmember extraction procedure and subsequent spectral unmixing of hyperspectral data. These are:

1. Currently, a majority of automatic endmember extraction algorithms assume the presence of pure pixels. For spaceborne hyperspectral data with a typical 30-m spatial resolution, it is very difficult to find pure pixels in rangeland ecosystem. A new technique that does not rely on the assumption of pure pixels is required to define meaningful endmembers for rangeland mapping.
2. Due to the spectral similarity between green vegetative species, it is very challenging to separate grasses from shrubs at peak mid-season growth.. Potential speparabitity may exist later in the season as shrub species remail green but most of the grasses will become senescent. Utilization of multi-temporal datasets may also be advantageous.

Given that the rangeland is highly heterogeneous, the spectral variability within the endmember classes is relatively high. New SMA procedures are required to handle the incomplete endmember set and incorporate this spectral variability within endmember classes in the spectral unmixing procedure.

ACKNOWLEDGEMENTS

We would like to acknowledge data provision and support from federal and provincial government and industry research partners, the Agriculture & Food Council, Alberta Sustainable Resource Development, Agriculture and Agri-Food Canada, Iunctus Geomatics and the University of Lethbridge.

REFERENCES

Asner, G.P. et al., 2002. Spectral unmixing of vegetation, soil and dry carbon cover in arid regions: comparing multispectral and hyperspectral observations. *International Journal of Remote Sensing*, 23, pp. 3939-3958.

Berman, M.; Kiiveri, H.; Lagerstrom, R.; Ernst, A.; Dunne, R.; Huntington, J. 2004. ICE: An automated statistical approach to identifying endmembers in hyperspectral images. *IEEE Transactions on Geoscience and Remote Sensing*, *42*, pp. 2085-2095.

Boardman, J. W.; Kruse, F. A.; Green, R. O. 1995. Mapping target signatures via partial unmixing of AVIRIS data. Summaries, Fifth JPL Airborne Earth Science Workshop, *JPL Publication 95-1*, vol. 1, pp. 23-26.

Chang, C.-I., Wu, C.-C., Liu, W.-W. and Ouyang, Y.-C., 2006. A new growing method for simplex-based endmember extraction algorithm. *IEEE Transactions on Geoscience and Remote Sensing*, *44*, pp. 2804-2819.

Gruninger, J. H.; Ratkowski, A. J.; Hoke, M. L. The sequential maximum angle convex cone (SMACC) endmember model. In: Shen, S. S.; Lewis, P. E., (Eds.), *Algorithms and Technologies for Multispectral, Hyperspectral, and Ultraspectral Imagery X, Proceedings of SPIE*, vol. 5425, Orlando, USA, **2004**, pp. 1-14.

Holechek, J. L. et al., 1989. Conservation, development and use of the world's rangelands. *Range Management Principles and Practices*, 501p.

Lass, L.W. et al., 2005. A review of remote sensing of invasive weeds and example of the early detection of spotted knapweed (Centaurea maculosa) and babysbreath (Gypsophila paniculata) with a hyperspectral sensor. *Weed Science*, 53, pp. 242-251.

Miao, L. and Qi, H., 2007. Endmember extraction from highly mixed data using minimum volume constrained nonnegative matrix factorization. *IEEE Transactions on Geoscience and Remote Sensing*, *45*, pp. 765-777.

Nascimento, J.M.P.; Dias, J.M.B. 2005. Vertex component analysis: a fast algorithm to unmix hyperspectral data. *IEEE Transactions on Geoscience and Remote Sensing*, *43*, pp. 898 – 910.

Neville, R. A.; Staenz, K.; Szeredi, T.; Lefebvre, J.; Hauff, P. Automatic endmember extraction from hyperspectral data for mineral exploration. In *Proceedings of Fourth International Airborne Remote Sensing Conference and Exhibition / 21st Canadian Symposium on Remote Sensing*, vol. 2. Ottawa, Canada, **1999**, pp. 891-897.

Neville, R., Sun, L. and Satenz, K. 2008. Spectral Calibration of Imaging Spectrometers by Atmospheric Absorption Feature Matching. *Canadian Journal of Remote Sensing*, in press.

Sun, L.; Neville, R.; Satenz, K. And White. H. 2008. Automatic Destriping of Hyperion Imagery based on Spectral Moment Matching. *Canadian Journal of Remote Sensing*, in press.

Staenz, K. and Williams, D.J., 1997. "Retrieval of Surface Reflectance from Hyperspectral Data Using a Look-Up Table Approach", *Canadian Journal of Remote Sensing*, 23, pp. 354–368.

Staenz, K., Neville, R.A., Levesque, J., Szeredi, T., Singhroy, V., Borstad, G.A. and Hauff, P., (1999. Evaluation of casi and SFSI hyperspectral data for environmental and geological applications - two case studies. *Canadian Journal of Remote Sensing*, 25, pp. 311-322.

Plaza, A.; Martinez, P.; Perez, R.; Plaza, J., 2004. A quantitative and comparative analysis of endmember extraction algorithms from hyperspectral data. *IEEE Transactions on Geoscience and Remote Sensing* , *42*, pp. 650-663.

Rowe, H.I. et al., 2002. Sustainable Rangelands Roundtable. *Rangelands*, 24, pp. 3-6.

Shimabukuro, Y.E.; and Smith, J.A., 1991. The least squares mixing models to generate fraction images derived from remote sensing on multispectral Data. *IEEE Transactions on Geoscience and Remote Sensing* , *29*, pp. 16-20

Winter, M. E. N-FINDR: An algorithm for fast autonomous spectral end-member determination in hyperspectral data. In: Descour, M. R.; Shen, S. S., (Eds.), Imaging Spectrometry V, *Proceedings of SPIE*, vol. 3753, 1999, Denver, USA. pp. 266–275.

Zhang, J., Rivard, B, and Rogge, D., 2008, The Successive Projection Algorithm (SPA), an Algorithm with a Spatial Constraint for the Automatic Search of Endmembers in Hyperspectral Data. *Sensors*, 8, pp 1321-1342.